

Modelling of the wall film in high-rate low liquid loading flows

Jørn Kjølås, SINTEF, Norway
Henning Holm, Equinor, Norway

ABSTRACT

In this paper we present a detailed analysis of large scale experimental data from the SINTEF Multiphase Laboratory on high-rate low liquid loading flows. The experimental work [1] was funded by Equinor as part of the Tanzania gas field development project [2] [3] [4], and SINTEF was granted access to use the data for improving the accuracy of the pressure drop predictions in LedaFlow. The experimental results showed that a key element for predicting high-rate low liquid loading flows accurately is to account for the droplets that deposit on the walls in the gas zone, creating a wall film. This wall film can have a profound effect on the hydraulic roughness experienced by the gas, and subsequently the frictional pressure drop. Furthermore, the data showed that this effect was particularly important for high liquid viscosities and in three-phase flows, and simulations showed that LedaFlow had a clear tendency to under-predict the pressure drop in such scenarios. To improve this situation, we used the data to derive a model for predicting this complex phenomenon. This paper summarizes the main parts of the data analysis and the development of the wall film model. We show that by introducing this new model into LedaFlow, we were able to significantly improve the agreement with the measurements.

1 INTRODUCTION

Low liquid loading generally refers to flow conditions where the superficial liquid velocity is small compared to the superficial gas velocity. This is a typical scenario for wet gas lines, where the reservoir produces mostly gas, but where changes in the pressure and temperature along the pipe causes condensation of water and hydrocarbons, so that the liquid rate increases with the distance from the well.

At gas high flow rates, one of the main challenges is to predict the pressure drop accurately, which in the presence of even tiny amounts of liquid can be challenging, as the pressure drop increases rapidly with increasing liquid rate. Also, Kjølås et al. [1] [5] showed that in three-phase low liquid loading flows at high gas rates, the pressure drop can depend significantly on the water cut. This can be clearly seen in Figure 1, which shows some of the data presented in [5]. We also observe in the same graph that the predictions obtained using LedaFlow 2.4 (solid lines) leaves something to be desired, as they are too low, especially in three-phase flows. The main reason for these discrepancies is that the wall in the gas zone is covered by a liquid film, which has a roughness that far exceeds the dry wall roughness. Indeed, a typical aspect of high rates low liquid loading flows is that droplets deposit on the walls in the gas zone, yielding a slow-moving liquid film on the pipe wall. The relatively high roughness of this film leads to an increase in flow resistance and ultimately higher pressure drop. Failure to account for this phenomenon properly in multiphase models can thus lead to considerable under-prediction of pressure drop, potentially leading to poor design decisions in new field developments and ultimately

reduced revenue. This matter is a particular concern in the Tanzania gas development project [3], where the produced fluids will be transported around 100 km to the receiving onshore facilities.

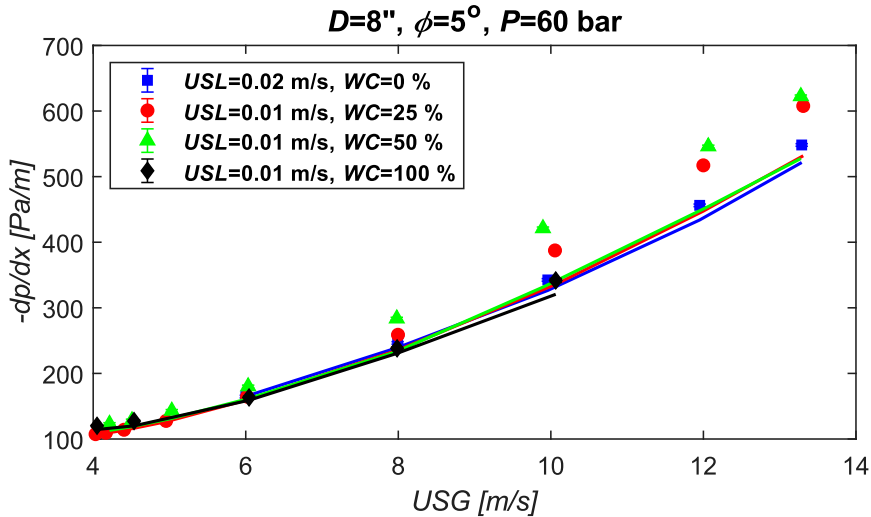


Figure 1: Pressure drop plotted against USG for experiments conducted in 2014 [5]. The lines are predictions obtained with LedaFlow 2.4.

The first rigorous model of the phenomenon of the wall film was presented by Laurinat et al. [6], who modelled the liquid distribution along the pipe perimeter by writing mass- and momentum conservation equations for the circumferential transport of the liquid along the wall. They concluded that droplet mass transfer through atomization and deposition was not sufficient to counteract gravitational drainage of the film. They thus argued that asymmetries in the film surface roughness cause secondary flow recirculation and give rise to circumferential interfacial stresses, which become significant for thin films near the top of the pipe.

A similar approach was later adopted by Bonizzi & Andreussi [7], who were able to obtain good agreement with measured film distributions by accounting for wave spreading in addition to droplet deposition and gravity. They also assumed a droplet deposition velocity model that was around an order of magnitude larger than that used by Laurinat et al..

More recently, Rodrigues et al. [8] constructed a wall film model based on the same principles as those used by Laurinat et al. [6] and Bonizzi & Andreussi [7]. However, they only considered the effect of gravity and droplet entrainment. They justified this by stating that other effects were most likely negligible in large diameter pipes, which was their target application area. They also assumed that the liquid concentration in the gas core decreased linearly with the distance from the interface. The latter assumption is unusual, as the concentration is known to (approximately) drop exponentially [9] [10] [11].

It seems clear from the work of these authors that predicting the liquid distribution accurately is challenging, especially if complex effects related to secondary flows and/or wave spreading are important. In this paper, we will therefore be employing a simpler approach to this modelling problem, where we do not attempt to resolve the full details of the wall film. Instead, we will assume that the wall film thickness is primarily driven by droplet entrainment and deposition on the wall, and that the action of gravity and secondary flows can be ignored. These assumptions are based on visual observations of wall films

obtained with high-speed video cameras, where we observe that the ripples on the film do not appear to have any preferred flow direction along the vertical axis. Also, in this work, it is not a goal in itself to have a very detailed representation of the wall film. Instead, the main goal is to predict the average roughness of the film, and thereby the frictional pressure drop. We therefore choose to focus on the aspects that are most important with this goal in mind, namely how the roughness of the film depends on the liquid properties and the flow conditions in the pipe. This will be discussed in more detail in section 3.

2 EXPERIMENTS

The experiments examined in this paper were conducted at the SINTEF Multiphase Flow Laboratory. The Large Scale Loop Facility was used and adapted with a 94 meter long 8" pipe, with an inclination angle 2.5° . A photograph of the experimental setup is shown in Figure 2. The nominal pressure was 60 bara, yielding a gas density of 67 kg/m^3 . The wall roughness of the pipe was determined to be approximately $45 \text{ }\mu\text{m}$ when completely dry (before any liquid had been introduced in the pipe), and about $30 \text{ }\mu\text{m}$ after the wall had been in contact with oil. For the experiments, nitrogen was used as the gas phase and Exxsol D60 as oil phase. For the aqueous phase, we used regular tap water with NaOH for corrosion protection, with and without glycerol. The purpose of adding glycerol was to increase the viscosity of the aqueous phase, emulating MEG injection. In the experiments with glycerol, the volumetric concentration was in the range 70-74%. The glycerol experiments were conducted at temperatures 23°C and 45°C yielding viscosities of about 42 and 14 cP, respectively, while the experiments without glycerol were conducted at 30°C . When changing the temperature, we also adjusted the pressure such that the gas density was kept the same in all the experiments.



Figure 2: Photograph of the experimental setup.

Table 1: Fluid properties at 60 bara

Density (Kg/m³)	Nitrogen @ 30°C	69.4
	Exxsol D60 @ 30°C	784
	Water @ 30°C	998.5
	Water+glycerol @ 23°C	1 197
	Water+glycerol @ 45°C	1 181
Viscosity (mPa s)	Nitrogen @ 30°C	0.018
	Exxsol D60 @ 30°C	1.3
	Water @ 30°C	0.8
	Water+glycerol @ 23°C	42
	Water+glycerol @ 45°C	14
Surface tension (mN/m)	Exxsol D60/Nitrogen @ 30°C	19
	Water/Nitrogen @ 30°C	64
	Water+glycerol/Nitrogen @ 23°C	52
	Water+glycerol/Nitrogen @ 45°C	52

For additional details on these experiments, we refer to Kjølås et al [1]. The experimental results will be shown in sections 4 and 5 in this paper along with the model predictions.

3 TWO-PHASE FLOW DATA ANALYSIS

As we observed in Figure 1, there is a need to improve the accuracy of the pressure drop predictions for LedaFlow in high-rate low liquid loading flows, and we believe that the main deficiency is in the gas-wall shear stress. Specifically, we believe that the main reason for the discrepancies between the predictions and the measured pressure drops is that the droplets that are generated at the gas-liquid interface at the bottom of the pipe deposit on the wall in the gas zone, and form a film which can have a roughness that is substantially higher than that of the dry wall. This is schematically illustrated in Figure 3. In the following sections we will analyse two-phase data with the aim of developing a model that predicts this phenomenon.

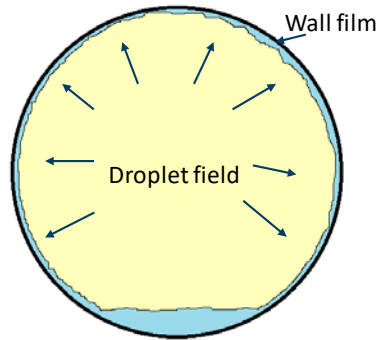


Figure 3: Illustration of the physical mechanism behind the wall film.

3.1 Estimation of the wall roughness in the gas zone

We have no direct measurements of the wall roughness or the film thickness in our experiments, we only have pressure drop measurements and density profiles obtained by scanning the pipe vertically with gamma densitometers. In principle, the gamma measurements could be used to deduce the thickness of the wall film, but unfortunately the

sensitivity of these instruments is too low for that. Consequently, we must use indirect methods to calculate reasonable values for the film roughness. Our method for doing this is straightforward: For each experiment, we select the gas-wall roughness that is needed for LedaFlow to match the measured pressure drop, and we infer that this is the average roughness of the wall in the gas zone. In other words, we assume that the closure laws used in LedaFlow for liquid-wall friction and interfacial friction are "correct". Obviously, these are rather bold assumptions, so we can therefore not always accept the prevailing results at face value, especially if the pressure drop is very sensitive to these other closure laws. However, given the measurements that we have at our disposal, it seems difficult to find a better way forward.

In Figure 4, we examine the sensitivity of the calculated roughness to the interface friction and the liquid-wall friction. The markers represent the estimated wall roughnesses, and the error bars show how much our estimates change when we vary the respective friction closure laws by $\pm 20\%$. By the looks of it, cases with $USL \geq 0.01$ m/s and $USG \geq 9$ m/s are arguably the most suitable cases, because the associated roughnesses are clearly above the baseline level of $30 \mu\text{m}$, and the error bars are typically less than $10 \mu\text{m}$.

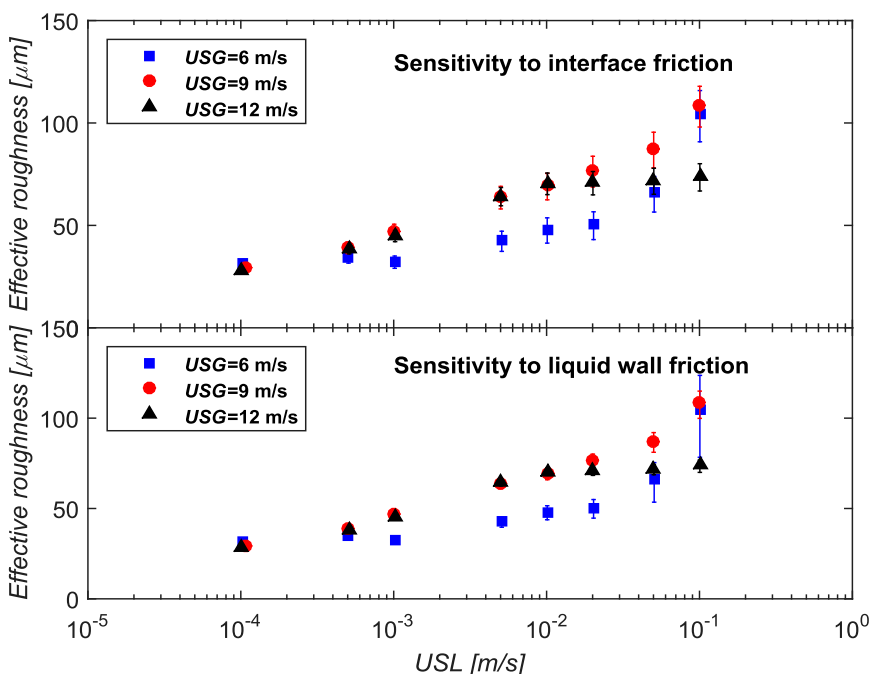


Figure 4: Experiments with Exxsol and Nitrogen at 60 bara pressure. The effective roughness has been computed by selecting the gas-wall roughness that is required to match the measured pressure drop with LedaFlow. The error bars show how much the optimal gas-wall roughness changes when the respective friction models (interface and liquid-wall) are multiplied with 0.8 and 1.2.

3.2 What determines the roughness of the wall film?

As we have pointed out, the key to predicting the pressure drop in high-rate low liquid loading flows is to predict the roughness of the film on the wall in the gas zone. This is a

problem that many authors have addressed, in particular with respect to vertical annular flows. We will mention a few of them here. Wallis [12] proposed that the interfacial friction coefficient for thin films can be represented by the following equation:

$$f_i = 0.005 \cdot \left(1 + 300 \frac{\delta}{D} \right) \quad (1)$$

where δ is the film thickness and D is the pipe diameter. Belt et al. [13] pointed out that Wallis did not subtract the contribution of the droplet momentum transfer when deriving this model, and thus derived a similar model where the droplet momentum contribution was removed:

$$f_i = 0.000683 \cdot \left(1 + 3393 \frac{\delta}{D} \right) \quad (2)$$

Rodrigues et al. [8] used a correlation on this form in their wall film model, except that they replaced the pre-factor with the gas-wall friction factor. Asali & Hanratty [14] proposed a somewhat similar friction factor correlation, but one that scales very differently with the gas density and pipe diameter:

$$f_i = f_g \cdot \left(1 + 0.045 (h_g^+ - 4) \right) \quad (3)$$

Here, f_g is the friction factor for the gas in the case of a smooth wall, and h_g^+ is defined as:

$$h_g^+ = \frac{\delta \cdot \rho_g \cdot u_{\tau g}}{\mu_g} \quad (4)$$

Here, ρ_g is the gas density, μ_g is the gas viscosity, and $u_{\tau g}$ is the friction velocity of the gas. Andreussi et al. [15] proposed a similar expression with slightly different coefficients, which Bonizzi & Andreussi applied in their wall film model [7]. Biberg et al. [16] proposed a model where they assumed that the hydraulic roughness k_S (as applied in the Colebrook friction factor formula [17]) equals a constant multiplied by the film thickness δ .

All of these approaches provide a relationship between the film thickness δ and the shear stress, hence to calculate the shear stress with these models, a value for the film thickness δ is needed. There happens to be a quite extensive literature on how to do that, with many different model proposals. In vertical low liquid loading flows, the film thickness is often thought to be limited by droplet entrainment [16], such that the film thickness equals the critical value where it becomes unstable, and where droplets are generated. This assumption transforms the problem of predicting the film thickness into a problem of predicting the local onset of droplet entrainment. Several authors suggest that the onset of entrainment in vertical flow coincides with the onset of disturbance waves [7] [18] [19] [20], and the onset of disturbance waves is usually thought to occur at some critical film Reynolds number. Ishii & Grolmes [21] suggest that the critical Reynolds number for disturbance waves is around 160, while Andreussi et al [15] proposed a correlation for the critical film Reynolds number, which depends on the viscosity ratio and the density ratio. A similar approach was also adopted by Owen & Hewitt [22]. We may also note that Biberg et al. [16] used a fixed value of 5000 for the critical Reynolds number for entrainment in vertical flow.

However, van Rossum et al. [23] showed experimental evidence that droplet entrainment could occur in vertical flow in the absence of disturbance waves if the gas velocity was sufficiently high. Consequently, the notion that the onset of entrainment and disturbance waves coincide is not necessarily correct. van Rossum et al. [23] proposed that the onset of entrainment for low film Reynolds numbers (outside the disturbance wave regime) was well correlated by a critical Weber number, defined as:

$$We_c = \frac{\rho_g u_g^2 \cdot \delta}{\sigma} = 17 \quad (5)$$

During the current development we tested many models for describing the liquid film on the wall, including those mentioned above, but with limited success. Specifically, the idea that the film thickness is given by some Reynolds number does not work for high liquid viscosities, because the film thickness then becomes unreasonably large. Therefore, we will now present a new approach to address the challenge of predicting the roughness of thin films. We start by making two basic postulates:

1. The hydraulic roughness k_S of a thin liquid film scales linearly with the size of the ripples d_{ripple} on the film: $k_S = K \cdot d_{ripple}$.
2. When the ripples on the film become sufficiently large, they are destroyed/atomized by the turbulent fluctuations in the gas. This limits the ripple size to the value d_{ripple}^{\max} .

Postulate 2 suggests that the maximum possible ripple size might be calculated in the same way as the maximum stable droplet size was calculated by Hinze [24], who argued that the maximum stable droplet size is given by a balance between the destructive forces of turbulence, and the stabilizing surface tension forces:

$$d_{ripple}^{\max} \propto d_{Hinze} \equiv 0.725 \left(\frac{\sigma}{\rho_g} \right)^{0.6} \varepsilon^{-0.4} \quad (6)$$

Here, ε is the energy dissipation rate per unit mass (m^2/s^3). This, combined with postulate 2 leads to:

$$k_S = K \cdot d_{Hinze} \quad (7)$$

In the next section we will test this simple idea.

3.3 A preliminary model for low liquid viscosities

For the purpose of testing the idea outlined in the previous section, we must select some suitable data. First, we wish to select data for which we are confident that the gas perimeter is completely covered by liquid, because that greatly simplifies the analysis. Secondly, we should for now select data with low liquid viscosities, because the droplet model developed by Hinze [24] does not work for elevated viscosities. The latter issue will be addressed in the next section.

Figure 5 shows a graph with the selected data, where we have plotted the effective wall roughness in the gas zone against the Hinze droplet diameter d_{Hinze} , see equation (6). The energy dissipation ε has been calculated as:

$$\varepsilon = \frac{S_g \tau_g u_g + S_i \tau_i \Delta u}{0.25 (S_g + S_i) \rho_g D_{hg}} \quad (8)$$

Here, S_g is the gas perimeter, τ_g is the gas-wall shear stress, S_i is the interface perimeter, τ_i is the interfacial shear stress, Δu is the gas-liquid slip velocity, and D_{hg} is the hydraulic diameter for the gas zone. These parameters were calculated using LedaFlow, as they are difficult to estimate from the available measurements. We have for the sake of simplicity assumed that the velocity of the wall film in the gas zone is zero.

The data points line up reasonably well, suggesting that there is indeed a linear relationship between the hydraulic roughness of the film k_S and d_{Hinze} , as we postulated in the previous

section. The black line in Figure 5 represents the relationship given by equation (7), where we have selected a value of 0.07 for the coefficient K .

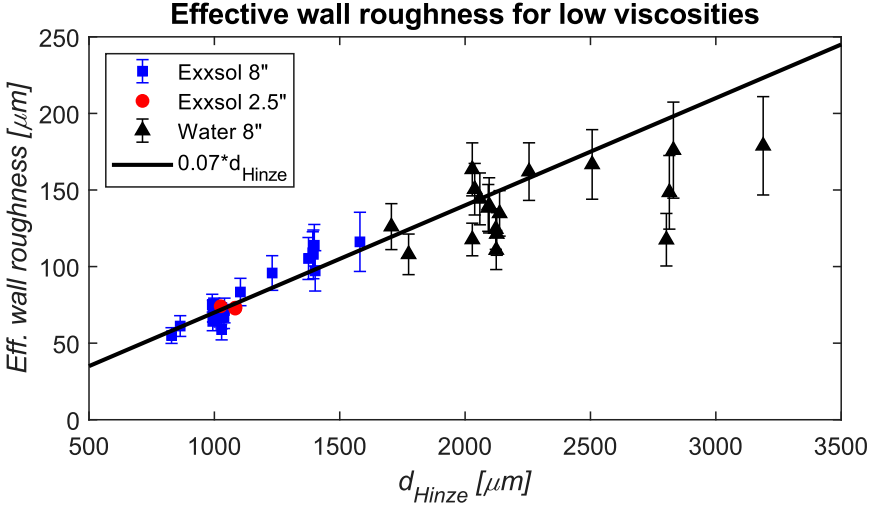


Figure 5: Effective wall roughness in the gas zone (calculated from pressure drop) plotted against the Hinze droplet diameter [24] for low-viscosity liquids ($\mu_L=0.8-1.5$ cP).

3.4 Generalization to high viscosities

Figure 5 only includes data in a very narrow viscosity range (0.8-1.5 cP). The reason for leaving out other viscosities was that we know that the size of droplets, and thus also the ripples on thin liquid films, depend on the viscosity. Therefore, the ratio between the effective roughness and the Hinze droplet diameter was never expected to be a fixed value. Specifically, increasing the viscosity of the droplets/ripples causes an increased resistance to the destructive turbulence forces, leading to larger maximum droplet/ripple sizes. Consequently, the Hinze droplet model, which does not depend on the droplet viscosity, will typically yield too small values for elevated viscosities.

Figure 6 shows an example illustrating the effect of the viscosity on the wall film ripples, where we compare pictures of the high-rate low liquid loading flows for three different viscosities (1.8, 33 and 90 cP). We observe here that the ripples are very small for the lowest viscosity (left picture), while they are considerably larger for the higher viscosities. Interestingly, the ripples for the highest viscosity do not appear to be larger than for the 33 cP oil.

A theoretical analysis of the effect of viscosity on droplet sizes was conducted by Arai et al. [25], who generalized the expression for the maximum droplet diameter by Hinze [24] to account for the droplet viscosity:

$$d_{\max} = C \cdot \left(\frac{\sigma \cdot f(Ca)}{\rho_g} \right)^{0.6} \varepsilon^{-0.4} \quad (9)$$

$$f(Ca) = 1 + k \cdot Ca \quad (10)$$

$$Ca = \frac{\mu_d (\varepsilon \cdot d)^{1/3}}{\sigma} \quad (11)$$

Here μ_d is the droplet viscosity. The function $f(Ca)$ could not be derived analytically, and was thus obtained by fitting empirical droplet size data extracted from stir tank experiments with oil and water. The authors pointed out that the maximum droplet size did not increase indefinitely with the viscosity in the stir tank experiments, like the model suggests. Instead it seemed to level off at a certain point. This observation appears to be in qualitative agreement with the pictures shown in Figure 6, where the ripples for the 90 cP oil are no larger than for the 33 cP oil. The authors reasoned that the cause of this was that when the viscosity became large enough, re-establishing the spherical form after deformation would be delayed by the viscous forces, allowing the turbulence to further deform already deformed droplets, facilitating the break-up process. The authors did however not attempt to model this phenomenon.

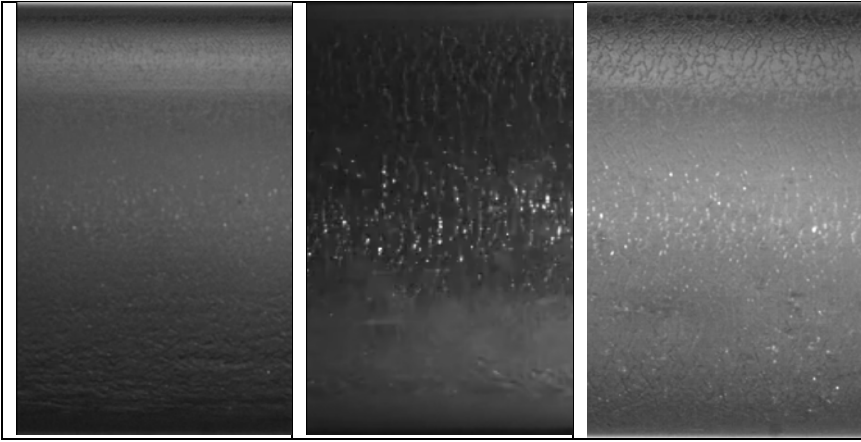


Figure 6: Snapshots of experiments with $USG=9$ m/s, $USL=0.1-0.2$ m/s and viscosities 1.8, 33 and 90 cP, respectively.

Since our wall film model is based on the same principles as droplet break-up in the presence of turbulence, it seems reasonable to generalize the wall film model in the same way that Arai et al. extended the droplet model by Hinze. When defining the capillary number Ca , it is not entirely clear which length scale we should use. However, this choice does not really matter as long as we can adjust the coefficient k based on our experimental data. Consequently, we simply use d_{Hinze} for calculating the value of the capillary number Ca . In equation (10), Arai et al. suggested a value for k equal to 9.0. It should however be mentioned that Arai et al. performed experiments by mixing oil and water in a beaker with an impeller, and in such a configuration the turbulence will not be completely isotropic. Consequently, some droplets would have experienced lower levels of turbulence than the average value, so that the maximum droplet size probably became larger than if the turbulence were isotropic. We therefore expect that their estimate of the coefficient k may be on the low side. In Figure 7 we show the ratio between the hydraulic roughness and d_{Hinze} as a function of the capillary number Ca , which we defined as:

$$Ca = \frac{\mu_d (\varepsilon \cdot d_{Hinze})^{1/3}}{\sigma} \quad (12)$$

The black dashed line is a model based on the analysis/observations by Arai et al.:

$$k_s = 0.052 \cdot \min[1 + 33 \cdot Ca, 6.6]^{0.6} \cdot d_{Hinze} \quad (13)$$

The only difference between this model and the preliminary low-viscosity model is that we have replaced the coefficient 0.07 by an expression containing the capillary number Ca . It should be noted that we have used a value of 33 for the coefficient k in equation (10), which is significantly higher than the value of 9.0 proposed by Arai et al. This difference might be partially explained by non-isotropic turbulence in the original experiments. In addition, we have assumed that the film on the wall has zero velocity, causing the coefficient to "absorb" the effect of the liquid viscosity on the liquid film velocity, which in reality is non-zero.

In Figure 7 we have included experiments conducted at Tiller in the 1980's with naphtha, in order to make sure that the model works for very low viscosities (naphtha has a viscosity of around 0.3 cP). The remaining data sets are from the Tanzania campaign [1].

We see that the data indicates that above a certain capillary number, the effective roughness stops increasing, which is qualitatively consistent with the observations by Arai et al. We account for this by introducing a cut-off in the viscosity correction term (the value 6.6 in equation (13)). We observe that some data points exceed this cut-off, but we ignore those points in order to keep the model simple. These points do however suggest that there may be some potential for improvement of this model for high capillary numbers, as the physical mechanisms at work here are presently not well understood.

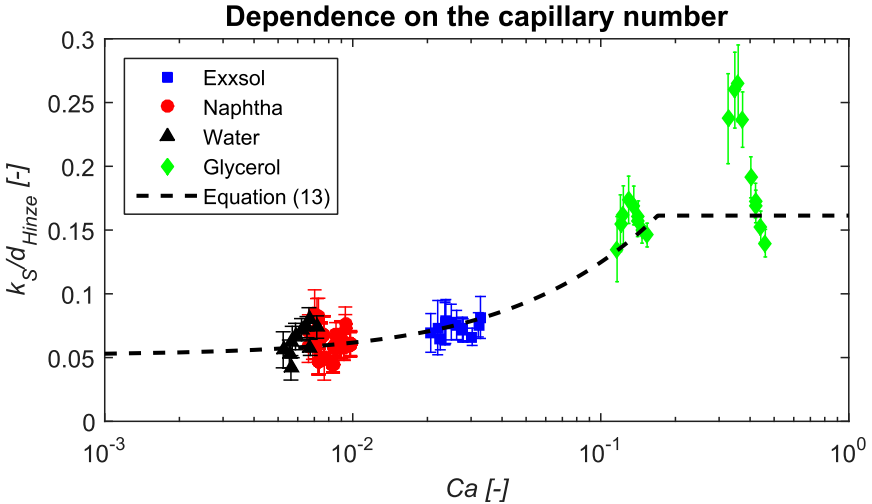


Figure 7: The ratio between the hydraulic roughness in the gas zone and the Hinze droplet size plotted against the capillary number for different liquids.

3.5 Accounting for the extent of the droplet field

So far we have focused on experiments with "annular flow", where the whole gas perimeter is covered by a liquid film, and we have for the sake of simplicity assumed that the wall film has a uniform roughness. In many scenarios, however, the droplet field does not extend all the way to the top, in which case the top of the pipe wall will remain practically dry. The reason for this is that gravity, in competition with turbulent diffusion, limits the vertical range of the droplets, yielding an asymmetric droplet field.

To account for this phenomenon, we use the existing droplet field model in LedaFlow. This model [10] calculates the droplet field from a diffusion-gravity equation, leading to a concentration profile that decreases exponentially with distance from the gas-liquid interface. Specifically, we postulate that when the predicted local concentration is below some critical (undisclosed) value, the pipe wall in that region can be considered "dry". On the other hand, if the predicted droplet concentration is above this critical value, we assume that the wall in that region is covered by a film with a roughness equal to that given by equation (13). If the droplet concentration does not fall below the critical value at any point along the vertical centreline of the pipe, then we assume that the entire gas perimeter is covered by a film, yielding annular flow.

Obviously, the situation is more complex than this, presumably with a more gradual transition between dry/wet walls. Specifically, the approaches used by Laurinat et al. [6] and Bonizzi & Andreussi [7] offer more refined pictures of the wall film, but those models also require the modelling of some very complex phenomena, such as secondary flows and wave spreading, and thus also necessitate the introduction of additional empirical correlations and model coefficients. Our assessment was that from a cost-benefit perspective, adding such complexity to the model was not warranted.

Basically, the underlying assumption in our approach is that when the droplet field is sufficiently dense, the wall film thickness is primarily governed by droplet deposition and entrainment, and that effects related to gravity and secondary flows/wave spreading are only of secondary importance. This simple approach that we have adopted here does however seem to qualitatively capture the effects that we observe, and thus appears adequate. This will be demonstrated in the next section.

Another aspect that needs to be addressed is that when the liquid film at the bottom of the pipe becomes very thin, it also becomes very narrow. Since this film is the source of the droplet field, the droplets need to travel laterally to deposit on the side walls, and if the lateral distance is very large, the droplets may not be able to reach the side walls. To account for this effect, we use a simple ad hoc correction which says that the width of the droplet field cannot be greater than some (undisclosed) constant multiplied with the width of the bottom film. If the width of the droplet field is smaller than the pipe diameter, we assume that the part of the wall outside this range is dry. This effect is however typically unimportant, unless the liquid rate is very small ($USL \leq 10^{-3}$ m/s).

4 VALIDATION OF THE TWO-PHASE MODEL

In this section we will test the model that we have outlined on two-phase gas-liquid flows. This model was implemented in LedaFlow 2.5, so refer to the new model as LedaFlow 2.5 in the remainder of this paper. It should be noted that the data that we present here does contain the data that we used to develop the model, so our use of the term "validation" may be somewhat debatable. We have however tested the model on many other data sets in addition to those that we show here, but for the sake of brevity, we limit the scope to include the Tanzania-data and some Tiller-experiments conducted with naphtha in the 1980's.

Figure 8 shows the normalized pressure drop plotted against USG for the different sets of liquid properties at $USL=0.01$ and 0.1 m/s. The markers represent measured values, and the dashed/solid lines represent predictions with the LedaFlow 2.4/2.5. We observe that LedaFlow 2.4 systematically under-predicts the pressure drop at these conditions, while the new model (LedaFlow 2.5) is in much better agreement with the measurements. In particular, we see that the new model is able to capture the trends related to both surface tension and viscosity, whereas the old model did not do that very well. For low/moderate gas rates, the discrepancies appear to be larger than at high rates. This is however mainly

because we are dividing the frictional pressure drop by a smaller value for those conditions, so the absolute deviations are not necessarily very large for those cases.

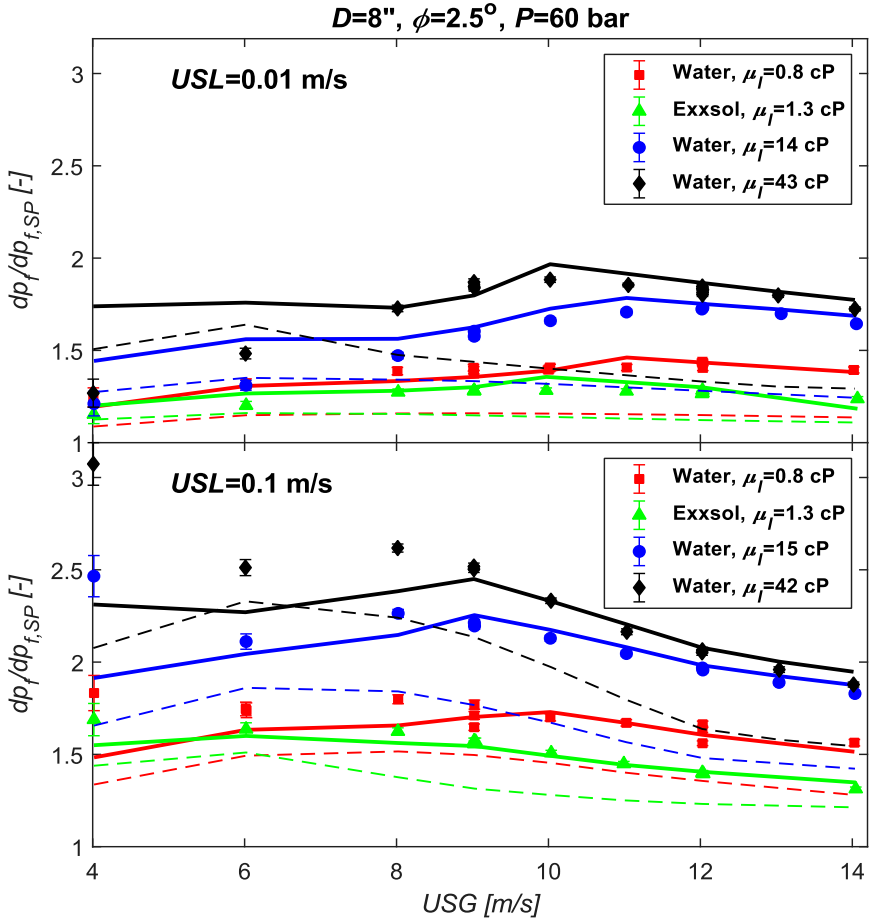


Figure 8: Pressure drop vs. USG for $USL=0.01$ and 0.1 m/s for four different liquids. The markers represent measured values, and the solid line represent predictions with the new model (LedaFlow 2.5). The dashed lines represent LedaFlow 2.4.

Figure 9 shows the pressure drop plotted against USL for $USG=9$ and 12 m/s. Just as in Figure 8, these plots also show that LedaFlow 2.4 (dashed lines) is consistently low on pressure drop in these conditions, and that the introduction of the new model in LedaFlow 2.5 (solid lines) improves the accuracy of the predictions. Again we see that the new model is able to reproduce the trends related to the thermodynamic properties of the liquid quite well.

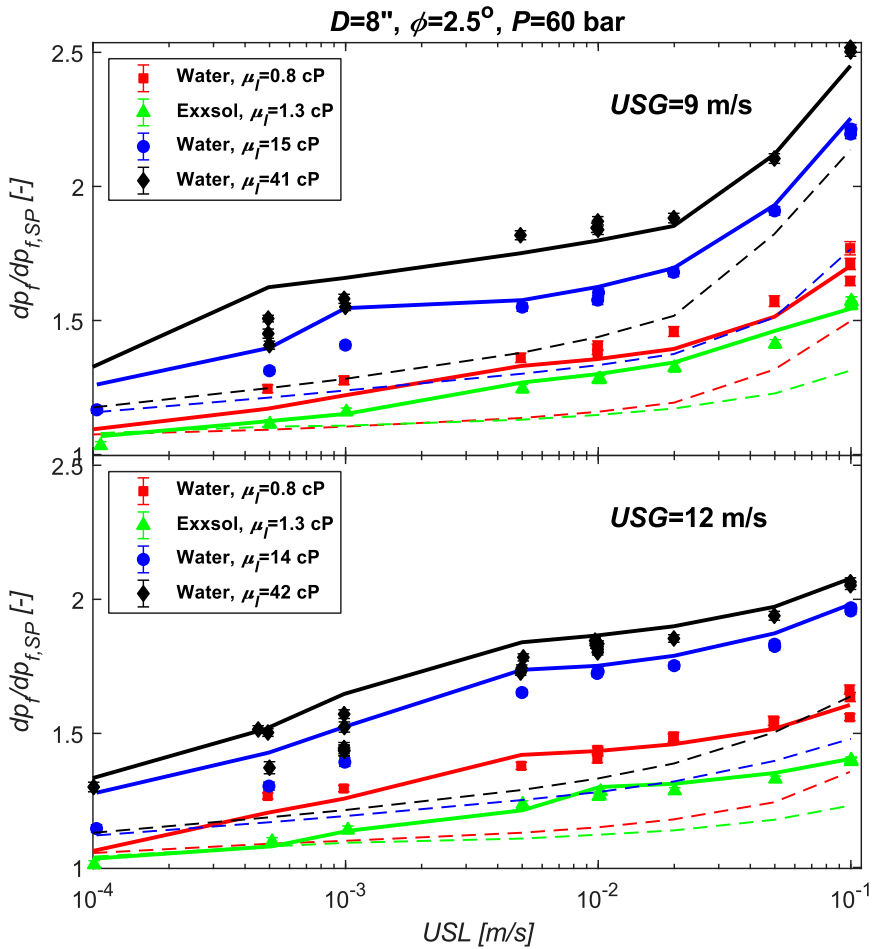


Figure 9: Pressure drop vs. USL for $USG=9$ and 12 m/s for four different liquids. The markers represent measured values, and the solid line represent predictions with the new model (LedaFlow 2.5). The dashed lines represent LedaFlow 2.4.

Figure 10 shows a set of graphs where we compare the predicted pressure drop with the measured values for various data sets (naphtha, Exxsol and water with and without glycerol). The graphs on the left represent simulation results obtained using LedaFlow 2.4, while the graphs on the right represent the new model (LedaFlow 2.5). The marker colour indicates the quality of the predictions. Specifically, green means that the predicted value is within 10% of the measurement, yellow implies a deviation between 10% and 20%, and red means a deviation greater than 20%. The distribution of green/yellow/red points are indicated as text in the graphs. It is clear from this plots that the agreement with data is significantly better with the new model. This is even the case for the naphtha experiments conducted at Tiller in the 1980's, where the predictions with LedaFlow 2.4 were already reasonably accurate.

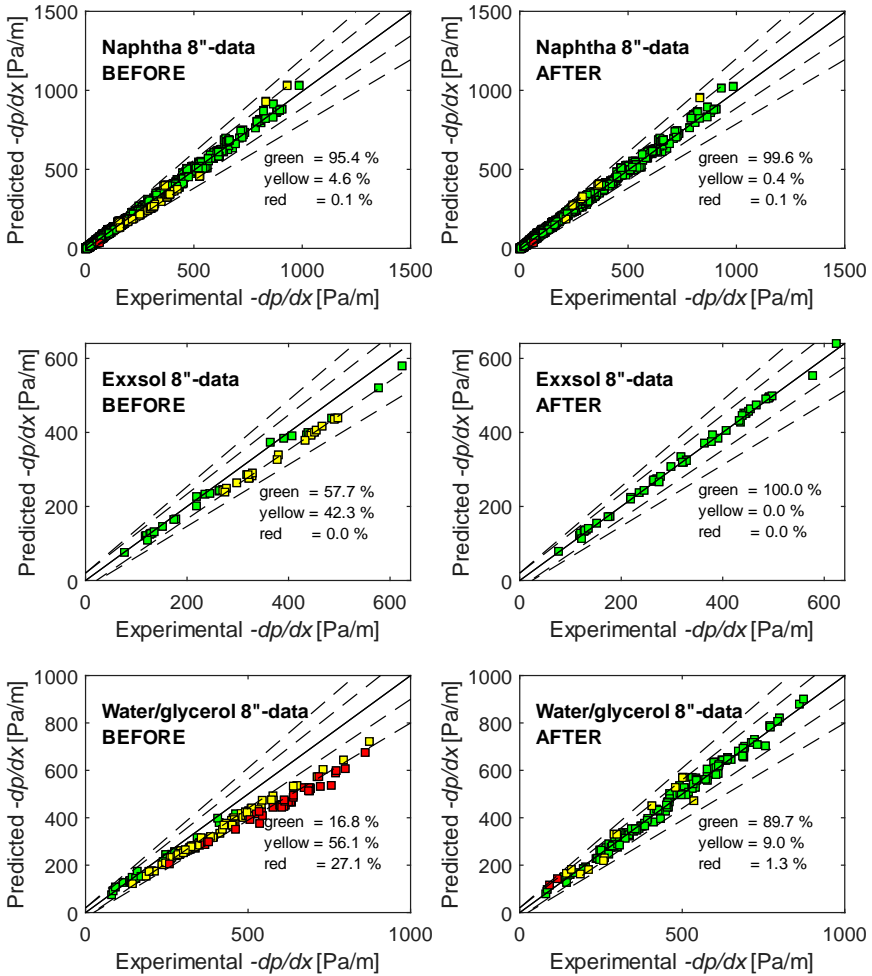


Figure 10: Predicted pressure drop plotted versus measured pressure drop for different data sets from campaigns conducted at Tiller: Naphtha-data from the 1980's, and the new Equinor-data used to develop the new model. The points that are within 10% of the measured value are given a green colour. The graphs on the left were generated with LedaFlow 2.4, and the graphs on the right were generated with LedaFlow 2.5.

5 GENERALIZATION TO THREE-PHASE FLOWS

In this section, we will extend the two-phase model that we outlined in section 3 to three-phase flows. In [1] it was argued that at the relatively high gas rates covered, the oil and water is probably completely mixed. The reasoning behind this assessment was that the pressure drop was found to be independent of the water properties at moderate water cuts, suggesting that the liquid flowed as an oil-continuous mixture with water droplets inside the oil. This simplifies the extension of the model to three-phase flows, because we can then more or less use the two-phase model as is: we just have to make some sensible assumptions with respect to the thermodynamic properties of the liquid mixture, which we may also apply to the wall film.

Schümann [26] showed that the viscosity of the liquid mixtures used in this campaign could be predicted quite adequately using the Brinkman emulsion model [27]. This model says that the relative viscosity of a liquid μ_{rel} containing suspensions (droplets) with some concentration ϕ , equals $\mu_{rel} = (1 - \phi)^{-2.5}$. In addition, it was found that the inversion point occurs approximately at the point where the (theoretical) effective viscosity of the oil-continuous mixture and the water-continuous mixture coincide.

In order to use the emulsion model on the wall film, we must assume some droplet concentration ϕ . Here, we simply assume that the water fraction in the wall film is equal to the global water cut. At a certain point, we did consider implementing a more advanced model to calculate the water fraction in the wall film based on local droplet concentration profiles. However, this effect was found to be quite marginal, so we elected to go with this simple approach instead.

The surface tension of the liquid mixture is a little difficult to assess, but it seems reasonable to assume that some areas of the wall film are oil-continuous, while other areas may be water-continuous. Consequently, the average value is probably somewhere in between the values for gas-oil and gas-water. The exact choice of this parameter did not appear to be critical, so we have chosen to use a simple arithmetic average of the values for gas-oil and gas-water, using the respective phase fractions α_o and α_w as weighting parameters:

$$\sigma_{gl} = \frac{\alpha_o \sigma_{go} + \alpha_w \sigma_{gw}}{\alpha_o + \alpha_w} \quad (14)$$

Finally, we found that the plateau introduced on the viscosity effect (the value 6.6 in equation (13)) did not appear to apply in three-phase flows, as the wall film roughness in three-phase experiments with glycerol-water clearly exceeded the proposed value. The reason for this may be that the dynamic behaviour of liquids with a dispersion-enhanced viscosity differs from that of pure liquids. Specifically, the physical explanation for this plateau in the first place was that the viscosity increased the restoration time of partially deformed ripples. Thus, our interpretation of this is that the presence of dispersed droplets might increase the effective viscosity without affecting the restoration time. To account for this observation, we treat the effect of the pure viscosity and the dispersion effect separately, only imposing a limit on the effect of the pure liquid viscosity. This leads to the following expression for the effective wall roughness k_s :

$$\left(\frac{k_s}{0.052 \cdot d_{Hinze}} \right)^{5/3} = \min(1 + 33 \cdot Ca, 6.6) + 33 \cdot \left(\frac{\mu_l^{eff}}{\mu_l^{pure}} - 1 \right) \cdot Ca \quad (15)$$

Here, we define the capillary number Ca as in equation (12), using the viscosity of the continuous liquid μ_l^{pure} , and not the effective viscosity μ_l^{eff} .

Figure 11 shows the normalized pressure drop plotted against the water cut for three different gas rates ($USG=6, 9$ and 12 m/s), and two different liquid rates ($USL=0.01$ and 0.1 m/s). Each graph contains data for one or more fluid systems (with/without glycerol), where the main distinguishing factor is the water viscosity. The markers in the graphs represent the measured values, while the lines are predictions. The dashed lines are predictions obtained with LedaFlow 2.4, and the solid lines are predictions by the new model (LedaFlow 2.5). We have used the Brinkman emulsion model [27] in both sets of simulations.

As expected, the predictions with the new model are significantly more accurate than those obtained with LedaFlow 2.4, where the predicted pressure drop is consistently too low. We

notice however that for the regular water, the maximum pressure drop occurs at a water cut close to 80%, while the model predicts that the maximum pressure drop occurs at a water cut of 50%. The predictions in the high water cut range are thus low compared to experiments for this fluid system. At first, it was believed that the source of this behaviour was that the average water fraction of the droplet field, and subsequently the water fraction in the wall film was much lower than the global value. Qualitatively, this makes sense because the water droplets are presumably larger and heavier than oil droplets, so that the water should be somewhat under-represented in the droplet field. However, when we attempted to incorporate this effect in the model, we observed some problems:

1. When modifying the water fraction in the wall film such that the maximum pressure drop occurred at a water cut of 80%, the predicted pressure drop for low water cuts became too low compared to the data for all fluid systems.
2. Reducing the water fraction of the wall film for the cases with glycerol caused the maximum pressure drop occur at too high water cuts for these fluid systems. This is not too surprising, since we observe that the predicted maximums are almost spot on already, without modifying the wall film water cut.

It is difficult to argue that the effect of the "slanted" wall film water fraction only applies to regular water, and not glycerol-water. If anything, one might expect a larger shift for the glycerol-water, which has a higher density than regular water. We therefore conclude that the apparent shift in inversion point that we see for the cases with regular water is probably not caused by a shift in the droplet field water fraction.

We believe that the main reason that the pressure drop increases beyond the 50% mark is that an oil-continuous emulsion forms on the wall. Normally, the emulsion should be mainly water-continuous at water cuts above 50% for regular water, at least according to the oil-water experiments [26]. We must however keep in mind that the emulsion on the wall is more or less static, while the liquids in the oil-water experiments are exposed to violent mixing. We have observed in earlier oil-water experimental campaigns that the emulsion layer in the separator can be largely oil continuous with very high water fractions (>90%). This happens because the oil drains out between the water droplets, but the water droplets are so stable that they do not coalesce without "assistance". Our hypothesis is that a similar phenomenon occurs on the wall in the gas zone in the three-phase experiments, i.e. that most of the oil migrates to the surface of the film, leaving behind water droplets that "should" coalesce to a continuous water film. However, the water droplets are partially hindered from coalescing because the oily interface between the water droplets is rendered virtually immobile, presumably by the presence of impurities/surfactants.

We should point out that for water cuts higher than 50%, the pressure drop for regular water is always lower than for viscous water. This makes sense because the flowing film at the bottom of the pipe is presumably water-continuous, and only the film on the wall in the gas zone is oil-continuous. The pressure drop thus increases with the water viscosity because of the water-continuous film at the bottom of the pipe.

This "delay" in phase inversion for the wall film is obviously difficult to predict, and it is certainly outside of the realm of hydrodynamic modelling, so we do not make any attempts to account for it here. It is also worth noting that a set of experiments where this inversion point shift was observed were later repeated (in a different project) using the same kind of fluid system, after the flow loop had been cleaned thoroughly. With the "clean" system, we observed that the maximum pressure drop occurred at a water cut around 50%, and not 80%. This largely corroborates the hypothesis that the inversion delay of the wall film is indeed caused by impurities that stabilize water droplets.

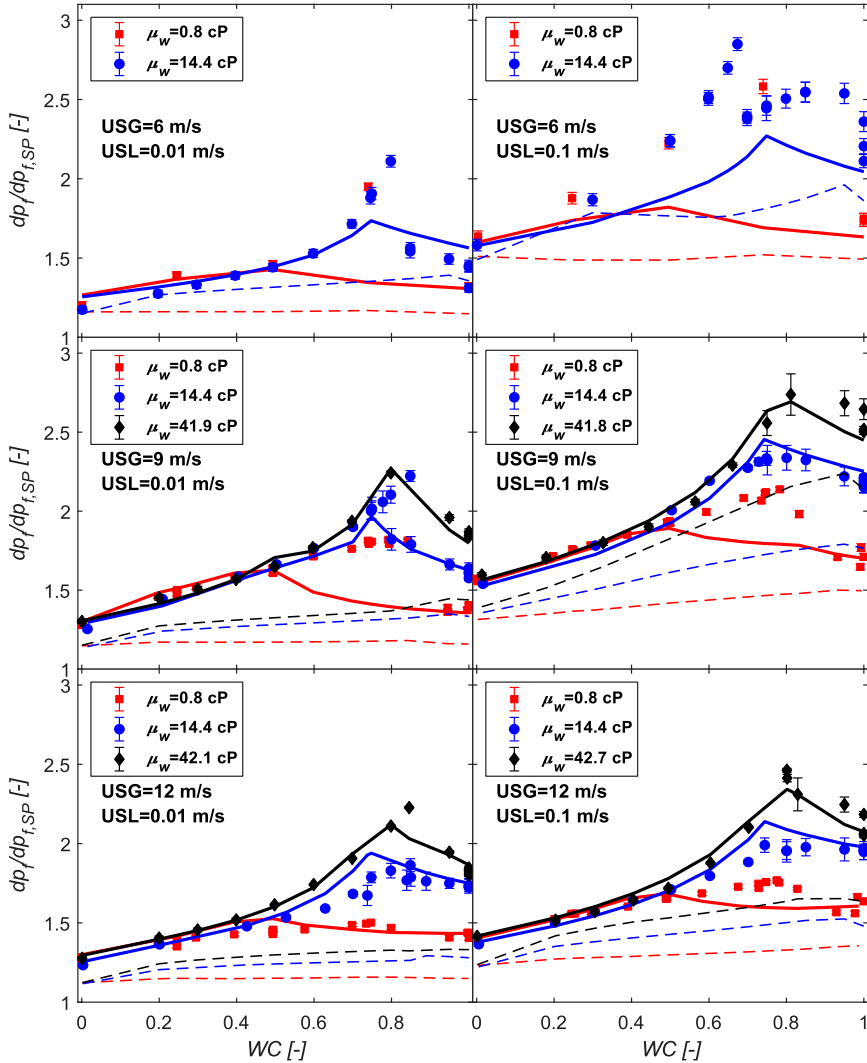


Figure 11: Normalized pressure drop plotted against the water cut for three different gas rates ($USG=6, 9$ and 12 m/s) and two different liquid rates ($USL=0.01$ and 0.1 m/s). The different colours represent the different water viscosities. The markers represent measured values, and the dashed/solid lines represent simulation results obtained with LedaFlow 2.4 and 2.5, respectively.

6 CONCLUSIONS

In near-horizontal multiphase gas-liquid flows at high gas rates, droplets are entrained from the film at the bottom of the pipe, and these droplets deposit on the walls in the gas zone, forming a wall film. This wall film modifies the hydraulic roughness experienced by the gas, and generally increases the frictional pressure drop. In this memo, we have analysed experimental data with low liquid rates and high gas rates in order to develop a model for predicting the extent and the effective roughness of the wall in the gas zone.

In the new wall film model, we assume that the hydraulic roughness of the film is proportional to the size of the ripples on the film. Furthermore, we assume that the size of the ripples are determined by the competition between destructive turbulence forces and the stabilizing forces of surface tension and viscosity. Using these assumptions, we formulated a model on the same form as the droplet size model proposed by Arai et al. [25].

By implementing this new wall film model in LedaFlow, we were able to obtain considerably better agreement with measurements in high-rate low liquid loading flows. The improvements were especially significant in scenarios with high liquid viscosities, and in three-phase flows.

7 ACKNOWLEDGEMENTS

The authors would like thank LedaFlow Technologies DA (co-owned by SINTEF, Kongsberg Digital, Total and ConocoPhillips) and the Research Council of Norway (project number 281881), for financing the model development described here, as well as this publication. We would also like to express our gratitude to the technical and scientific personnel at Tiller for their considerable efforts during the experimental campaign. Finally, we wish to thank Equinor and the Tanzania Gas Development Project - Block 2 for allowing SINTEF to use the Tanzania-data for improving LedaFlow, and for approving this publication.

8 REFERENCES

- [1] J. Kjølås, “Large scale experiments on high-rate three-phase low liquid loading flows,” in *18th International Conference on Multiphase Production Technology*, Cannes, 2019.
- [2] H. Holm, “Tanzania gas development - flow assurance challenges,” in *BHRG*, Cannes, 2015.
- [3] H. Holm, “Tanzania Flow Assurance Challenges updated,” in *BHRG*, Cannes, 2017.
- [4] H. Holm, “Tanzania Flow Assurance Challenges (Equinor ASA),” in *BHRG*, Cannes, 2019.
- [5] J. Kjølås, T. E. Unander, M. Wolden, A. Shmueli and H. Holm, “Pressure drop measurements in low liquid loading three-phase flows,” in *17th International Conference on Multiphase Production Technology*, Cannes, 2017.
- [6] J. Laurinat, T. Hanratty and W. Jepson, “Film thickness distribution for gas–liquid annular flow in a horizontal pipe,” *PCH Physicochem. Hydrodyn.*, vol. 6, p. 179–195, 1985.
- [7] M. Bonizzi and P. Andreussi, “Prediction of the liquid film distribution in stratified-dispersed gas–liquid flow,” *Chemical Engineering Science*, vol. 142, p. 165–179, 2016.
- [8] H. Rodrigues, E. Pereyra and C. Sarica, “A model for the thin film friction factor in near-horizontal stratified-annular transition two-phase low liquid loading flow,” *International Journal of Multiphase Flow*, vol. 102, pp. 29-37, 2018.
- [9] S. Paras and A. Karabelas, “Droplet entrainment and deposition in horizontal annular flow,” *Int. J. Multiphase Flow* 17, vol. 17, p. 455–468, 1991.

- [10] J. Kjølås, S. T. Johansen, Y. Ladam, R. Belt, T. J. Danielson and M. Stinessen, "Modeling of the droplet field in near-horizontal low liquid loading flows," in *BHRG*, Cannes, 2011.
- [11] R. Skartlien, S. Nuland and J. E. Amundsen, "Simultaneous entrainment of oil and water droplets in high Reynolds number gas turbulence in horizontal pipe flow," *International Journal of Multiphase Flow*, vol. 37, p. 1282–1293, 2011.
- [12] G. Wallis, *One-dimensional Two-phase Flow*, New York: McGraw-Hill, 1969.
- [13] R. J. Belt and L. M. Portela, "Prediction of the interfacial shear-stress in vertical annular flow," *International Journal of Multiphase Flow*, vol. 35, no. 7, p. 689–697, 2009.
- [14] J. Asali and T. Hanratty, "Interfacial Drag and Film Height for Vertical Annular Flow," *AIChE Journal*, vol. 31, no. 6, pp. 895-902, 1985.
- [15] P. Andreussi, J. Asali and T. Hanratty, "Initiation of roll waves in gas–liquid flows," *AIChEJ*, vol. 31, p. 119–126, 1985.
- [16] D. Biberg, C. Lawrence, G. Staff and H. Holm, "Pressure drop in low liquid loading flows - the effect of a thin liquid film on the pipe wall," in *BHRG*, Cannes, France, 2017.
- [17] C. F. Colebrook, "Turbulent Flow in Pipes, With Particular Reference to the Transition Region Between the Smooth and Rough Pipe Laws," *J. Inst. Civ. Eng.*, vol. 11, no. 4, pp. 133-156, 1939.
- [18] B. Azzopardi, "Drops in annular two-phase flow," *Int. J. Multiphase Flow*, vol. 23, pp. 1-53, 1997.
- [19] C. Berna, A. Escrivá, J. Muñoz-Cobo and L. Herranz, "Review of droplet entrainment in annular flow: Interfacial waves and onset of entrainment," *Progress in Nuclear Energy*, vol. 74, pp. 14-43, 2014.
- [20] T. J. Hanratty and A. Hershman, "Initiation of Roll Waves," *AIChE Journal*, vol. 7, no. 3, pp. 488-497, 1961.
- [21] M. Ishii and M. A. Grolmes, "Inception Criteria for Droplet Entrainment In Two-Phase Concurrent Film Flow," *AIChE Journal*, vol. 21, no. 2, pp. 308-318, 1975.
- [22] D. Owen and G. Hewitt, "An improved annular two-phase flow model.," in *The Third International Conference on Multiphase Flow*, the Hague, the Netherlands., 1987.
- [23] J. J. v. Rossum, "Experimental Investigation of Horizontal Liquid Films," *Chem. Eng. Sci.*, 11,35 (), vol. 11, no. 1, pp. 35-52, 1959.
- [24] J. O. Hinze, "Fundamentals of the hydrodynamic mechanism of splitting in dispersion process," *AIChE*, vol. 289, no. 1, 1955.
- [25] K. Arai, M. Konno, Y. matunaga and S. Saito, "Effect of Dispersed-phase viscosity on the maximum stable drop size for break up in turbulent flow," *Journal of chemical engineering of Japan*, vol. 10, no. 4, 1977.
- [26] H. Schümann, J. Kjølås, M. Wolden, C. Lawrence and H. Holm, "Rheology study: Comparison of a real condensate-MEG system and a model fluid system used in the Tiller Low-Liquid-Loading campaigns," in *18th International Conference on Multiphase Production Technology*, Cannes, 2019.
- [27] H. Brinkman, "The viscosity of concentrated suspensions and solutions," *J. Chem. Phys.*, vol. 20, no. 4, pp. 571-584, 1952.
- [28] Emerson. [Online]. Available: <http://www.emerson.com/en-us/automation/micro-motion>.

- [29] G. Chupin, "An Experimental Investigation of Multiphase Gas-Liquid Pipe Flow at Low Liquid Loading," NTNU, Trondheim, 2003.
- [30] H. Karami, C. F. Torres, E. Pereyra and C. Sarica, "Experimental Investigation of Three-Phase Low-Liquid-Loading Flow," in *SPE Annual Technical Conference and Exhibition*, Houston, 2016.
- [31] H. K. Dong, "Low Liquid Loading Gas-Oil-Water Flow in Horizontal Pipes- MS Thesis," The university of Tulsa, Tulsa, Oklahoma, 2007.
- [32] G. F. Hewitt, "Three-phase gas-liquid-liquid flows in the steady and transient states," *Nuclear Engineering and Design*, vol. 235(10-12), pp. 1303-1316, 2005.
- [33] B. Azzopardi, "Drops in annular two-phase flow," *Int. J. Multiphase Flow*, vol. 23, pp. 1-53, 1997.